A novel material-balance approach for estimating in-place volumes of gas and water in gas reservoirs with aquifer support

K. Jongkittinarukorn[1] · C. S. Kabir[2]

Abstract
Applications of the traditional static material-balance method in gas reservoirs become a challenge with production maturity due to variability in aquifer influx, infill drilling, and production-operational changes in offset wells, among others. Besides, some existing modeling approaches involve a trial-and-error method, making the solution outcomes nontrivial. This study proposes a new methodology for analyzing production data involving water-drive gas reservoirs. The main findings of this study include the following: (1) A straight-line plot that yields gas and water in-place volumes, (2) A modified-$(p_{av}/z)^*$ plot exhibits a straight-line with an x-intercept of gas initially-in-place, similar to that in a conventional-(p_{av}/z) plot, (3) A new definition of degree of aquifer support that is quantifiable using production data. Synthetic data verified the proposed modeling approach, whereas a field dataset provided validation.

List of symbols

B_g	Gas formation volume factor, RB/scf
B_w	Water formation volume factor, RB/STB
c_f	Formation compressibility, psi^{-1}
c_w	Water compressibility, psi^{-1}
D_{as}	Degree of aquifer support, dimensionless
E_a	Expansion of aquifer, RB/STB
E_{fw}	Cumulative expansion of connate water and reduction in the reservoir-pore volume, RB/scf
E_g	Cumulative expansion of gas, RB/scf
F	Fluid withdrawal volume, RB
G	Gas initially-in-place, scf
G_a	Apparent gas initially-in-place, scf
G_p	Cumulative gas production, scf
I_{CD}	Compaction-drive index, dimensionless
I_{GD}	Gas-drive index, dimensionless
I_{WD}	Water-drive index, dimensionless
J_g	Gas productivity index, MMscf-cp/D-psi^2
n	Number of production data points
p_{av}	Average reservoir pressure in a gas reservoir with aquifer, psia
p^*	Average reservoir pressure in a gas reservoir without aquifer, psia
S_{gr}	Residual gas saturation, %
S_{wi}	Irreducible water saturation, %
V_{ba}	Bulk volume of an aquifer, RB
V_{bap}	Predicted bulk volume of an aquifer, RB
V_{bg}	Bulk volume of a gas reservoir, RB
V_{bgp}	Predicted bulk volume of a gas reservoir, RB
V_{cw}	Volume of connate water, RB
V_{cwf}	Volume of connate water in a water-influx zone, RB
V_{cwg}	Volume of connate water in a gas reservoir, RB
V_f	Bulk volume of a water-influx zone, RB
V_g	Volume of gas in a gas reservoir, RB
V_{rg}	Volume of residual gas in a water-influx zone, RB
V_{wa}	Volume of water in an aquifer, RB
V_{wf}	Volume of aquifer water in a water-influx zone, RB
W	Water initially-in-place, STB
W_e	Cumulative water in flux, RB
W_p	Cumulative water production, STB
z	Gas deviation factor, dimensionless

Greek

ε	Error in V_{bg} estimation, RB
Δ	Change
ϕ	Porosity, fraction

Subscript

av	Average
i	Initial condition

✉ K. Jongkittinarukorn
drkittiphong@gmail.com

1 Chulalongkorn University, Bangkok, Thailand

2 Incendium Technologies, Inc., Round Rock, Texas, USA

🌀 Springer

Introduction

Reservoir engineers have relied on the material-balance equation or MBE to estimate gas initially-in-place (G). Some of the landmark studies, particularly those of Havlena and Odeh (1963), Cole (1969), and Campbell and Campbell (1978), developed tools for a water-drive gas reservoir. The presence of aquifer support increases the number of unknowns. This challenge of solving the gas MBEs appears in Bruns et al. (1965), Chierici et al. (1967), Dake (1983), Tehrani (1985), and Vega and Wattenbarger (2000), among others. Bruns et al. (1965) and Agarwal et al. (1965) have documented the effects of water influx on the (p_{av}/z) plot.

Specifically, Bruns et al. (1965) used various aquifer models, those of Schilthuis (1936), Hurst simplified (1943), and van Everdingen and Hurst (1949). Decades later, Elahmady et al. (2007) showed a non-uniqueness problem, leading to an overestimation of in-place gas volume, G. This issue arises due to the time-dependent nature of the aquifer influx model. To that end, Izgec and Kabir (2010) showed that a simplified form of the van Everdingen and Hurst aquifer-influx model could discern the variable nature of aquifer influx.

Yildiz and Khosravi (2007) showed the performance of their analytical tools in edge-water and bottom-water-drive systems. In a follow-up study, Yildiz (2008) offered a hybrid approach involving a modified version of the Roach (1981) plot and the McEwen (1962) method to ascertain in-place gas volume with production data in water-drive reservoirs. The illustrative examples supported the goodness of this methodology, particularly in strong water-drive systems. Some of the studies in the modern era include those of Moghadam et al. (2011), exploring the

application of the p/z method in coalbed-methane, over-pressured, and water-drive reservoir systems. Wang and Teasdale (1987) established the material balance equation (MBE) for a fractured vuggy gas reservoir with a bottom-water drive, including stress sensitivity and gravity segregation. The proposed MBE can be applied to estimate the original gas-in-place and the distribution of the reserve in the matrix, fracture, and cavity.

More recently, Yu et al. (2019) showed that the Blasingame method and the flowing-material balance (FMB) approach could lead to visual identification and analysis of the early aquifer-influx period data. Yu et al. (2019) proposed no–aquifer influx period-type curves and early aquifer–influx period-type curves, which can be applied to determine reservoir and aquifer parameters. Well history production data are divided into three influx periods: no-aquifer, early aquifer, and middle-late aquifer. It yields the dimensionless drainage radius, initial gas-in-place, other reservoir parameters, and aquifer energy. Also, Kazemi and Ghaedi (2020) presented a semi-analytical method for the FMB for edge-water-drive systems with reservoir pressure exceeding 3000 psi. For lower pressures, it requires a correction factor. Zaremoayedi et al. (2022) proposed a new production data analysis approach by applying a modified compressibility parameter to the conventional FMB equations to estimate the initial gas in place accurately and average reservoir pressure in a non-volumetric naturally fractured gas condensate reservoir. Without using complex multi-phase reservoir modeling, they modified the isothermal rock compressibility factor to model the aquifer's influence on reservoir performance.

Despite the plethora of studies in literature, aquifer volume (W_e) estimation becomes a challenge due to the uncertainty affecting the microscopic displacement efficiency and the conformance factor, as Chierici et al. (1967) pointed out. None of the previous works show a straight-line analysis. This study aims to develop a new methodology for a water-drive gas reservoir to estimate the aquifer volume during the boundary-dominated flow period. Our ultimate objective is to create a holistic modeling approach, given the challenges in the modern era involving complex fluid PVT, overpressured reservoirs, and aquifer influx. This investigation develops a modified-(p_{av}/z)* plot handling the variable water-drive situation and quantifies various degrees of aquifer support in a conventional reservoir. Estimations of gas and aquifer in-place volumes became the underlying motivation, given that this item has remained unexplored. Of course, the knowledge of aquifer strength associated with each well helps develop a reservoir's depletion strategy.
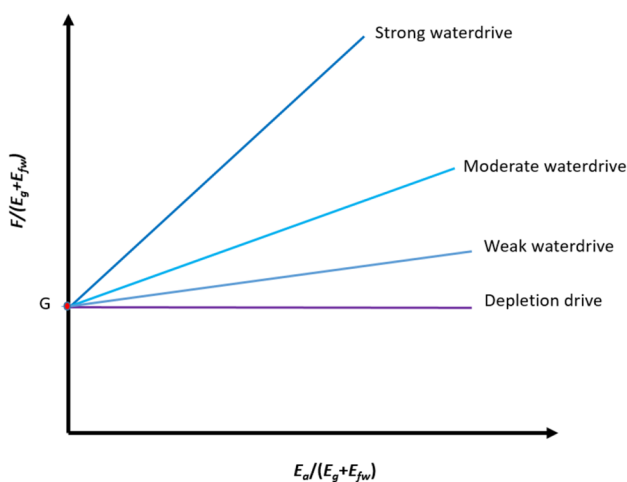

Fig. 1 A straight-line plot for a water-drive gas reservoir

Proposed methodology

Material balance equation in a water-drive gas reservoir

Let us write the material balance equation of a water-drive gas reservoir as

$$F = G(E_g + E_{fw}) + WE_a \tag{1}$$

where the fluid withdrawal (F), the cumulative expansion of gas (E_g), the incremental expansion of the connate water and reduction in the reservoir-pore volume (E_{fw}), and the cumulative expansion of water (E_a) are defined, respectively, as the following:

$$F = G_p B_g + W_p B_w \tag{2}$$

$$E_g = B_g - B_{gi} \tag{3}$$

$$E_{fw} = \frac{B_{gi}(c_f + S_{wi}c_w)\Delta p}{(1 - S_{wi})} \tag{4}$$

$$E_a = B_{wi}(c_w + c_f)\Delta p \tag{5}$$

W is water initially-in-place. While the classical gas MBE uses W_e, Eq. 1 uses W. Dividing Eq. 1 by $(E_g + E_{fw})$ and rearranging yields the following expression:

$$\frac{F}{(E_g + E_{fw})} = W * \frac{E_a}{(E_g + E_{fw})} + G \tag{6}$$

A dimensionless plot of $F/[E_g + E_{fw}]$ vs. $E_a/[E_g + E_{fw}]$, as illustrated in Fig. 1, yields a straight line with a slope of W
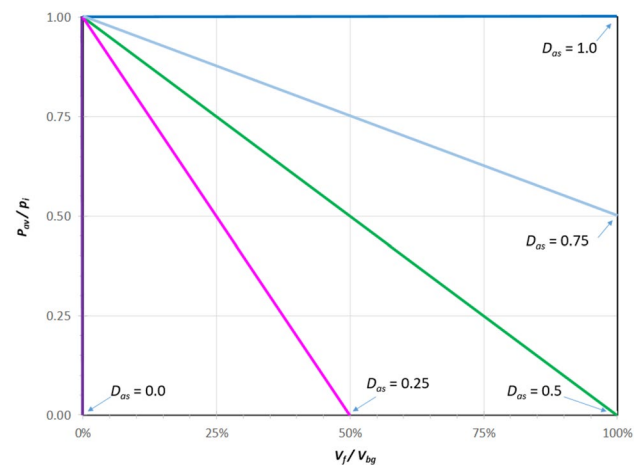

Fig. 2 Dimensionless reservoir pressure (p/p_i) vs dimensionless volume of a water-influx zone (V_f/V_{bg})

and G from the intercept. The larger the aquifer, the steeper the slope of a straight line. However, the y-intercept is independent of an aquifer's size. While both a straight-line plot and Cole plot yield the same y-intercept of G, this study offers straight-line profiles. Given that reservoir connectivity is a critical parameter not explicitly considered, Fig. 1 cannot assess the correct aquifer size. So, this index implies the relative contribution of water influx in the context of the drive mechanism.

Once G and W are known, the bulk volumes of a gas reservoir (V_{bg}), an aquifer (V_{ba}), and a water-influx zone (V_f) can be calculated, respectively, as

$$V_{bg} = \frac{GB_{gi}}{(1 - S_{wi})\emptyset_i} \tag{7}$$

$$V_{ba} = \frac{WB_{wi}}{\emptyset_i} \tag{8}$$

$$V_f = \frac{G_p B_g - V_{bg}\emptyset_i\left[(1 - S_{wi})\left(\frac{B_g}{B_{gi}} - 1\right) + (S_{wi}c_w + c_f)\Delta p\right]}{\emptyset_i\left[(1 - S_{gr})(1 - c_f\Delta p) - S_{wi}(1 + c_w\Delta p)\right]} \tag{9}$$

Correction for the (p_{av}/z) plot

A p_{av}/z plot of a water-drive-gas reservoir deviates from a straight line because of the presence of an aquifer. A part of a gas reservoir with a volume of V_{wf} represents the aquifer water. Without an aquifer, this volume gets filled with gas. Then, gas-pore volumes for models with and without aquifer are ($V_g + V_{rg}$) and ($V_g + V_{rg} + V_{wf}$), respectively. V_g is the volume of gas in a gas reservoir, and V_{rg} is the residual gas volume in a water-influx zone. Therefore, the average reservoir pressure of a model without an aquifer (p^*) should be lower than that for an aquifer (p). The value of p is corrected to p^* using the real-gas law. Then, the (p_{av}/z)* relation becomes

$$\left(\frac{p_{av}}{z}\right)^* = \left(\frac{p_{av}}{z}\right)\frac{(V_g + V_{rg})}{(V_g + V_{rg} + V_{wf})} \tag{10}$$

The values of V_g, V_{rg}, and V_{wf} can be estimated using the following equations:

$$V_g = (V_{bg} - V_f)\emptyset_i[1 - S_{wi} - (S_{wi}c_w + c_f)\Delta p] \tag{11}$$

$$V_{rg} = V_f\emptyset_i S_{gr}[1 - c_f\Delta p] \tag{12}$$

$$V_{wf} = V_f\emptyset_i\left[(1 - S_{gr})(1 - c_f\Delta p) - S_{wi}(1 + c_w\Delta p)\right] \tag{13}$$

Similar to the conventional (p_{av}/z) plot, a plot of (p_{av}/z)* vs. G_p yields a straight line with y-intercept $= (p/z)_i$ and x-intercept
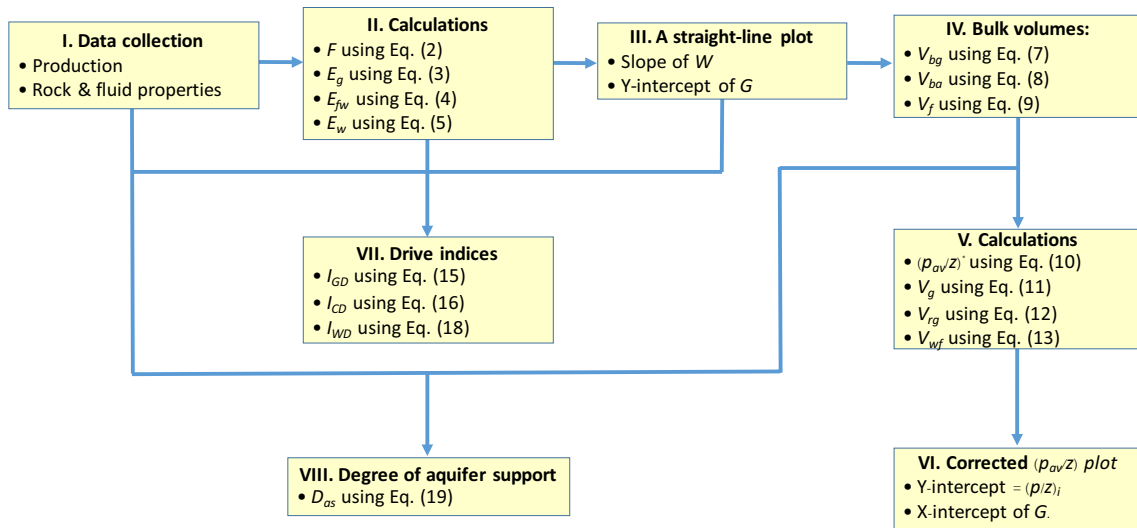
Fig. 3 Flowchart of the proposed methodology

Table 1 Rock and fluid properties for Example 1

Parameter	Value
ϕ, %	20
k, md	200
S_{wi}, %	20
p_i, psia	17,310
Gas SG	0.56
G, Bscf	115

Fig. 4 Production data for Example 1

of G. Note that this plot requires prior knowledge of gas in place which can be estimated from Fig. 1. The real objective of this section is to verify whether the value of G is correctly estimated.

Drive indices

Following Pletcher's pot aquifer (2002) definition of drive indices, let us rewrite Eq. 1 as

$$I_{GD} + I_{CD} + I_{WD} = 1 \tag{14}$$

where gas-drive index (I_{GD}), compaction-drive index (I_{CD}), and water-drive index (I_{WD}) are defined, respectively, as

$$I_{GD} = \frac{GE_g}{G_p B_g} \tag{15}$$

$$I_{CD} = \frac{GE_{fw}}{G_p B_g} \tag{16}$$

$$I_{WD} = \frac{\left(WE_a - W_p B_w\right)}{G_p B_g} \tag{17}$$

While Pletcher (2002) used W_e in I_{WD}, this study uses (WE_a). Quality of production data, reservoir complexity, infill drilling, and operational activities may pose challenges for Eq. 14. So, Kabir et al. (2016) recommended that I_{WD} gets evaluated using the following expression:

$$I_{WD} = 1 - I_{GD} - I_{CD} \tag{18}$$

Degree of aquifer support

Two dimensionless variables assisted in quantifying the degree of aquifer support, D_{as}. Let us define D_{as} within a range of 0 and 1; zero implies no energy support, whereas
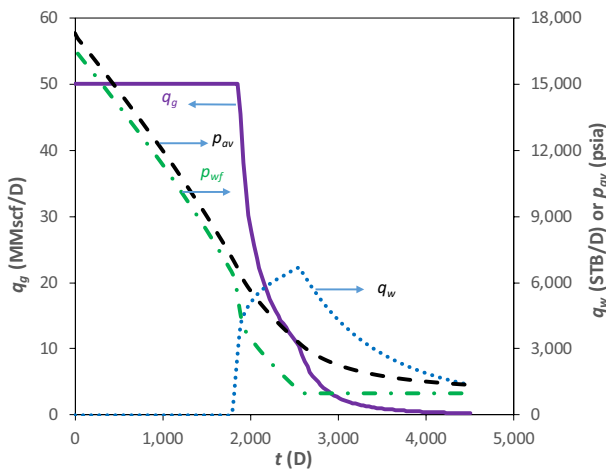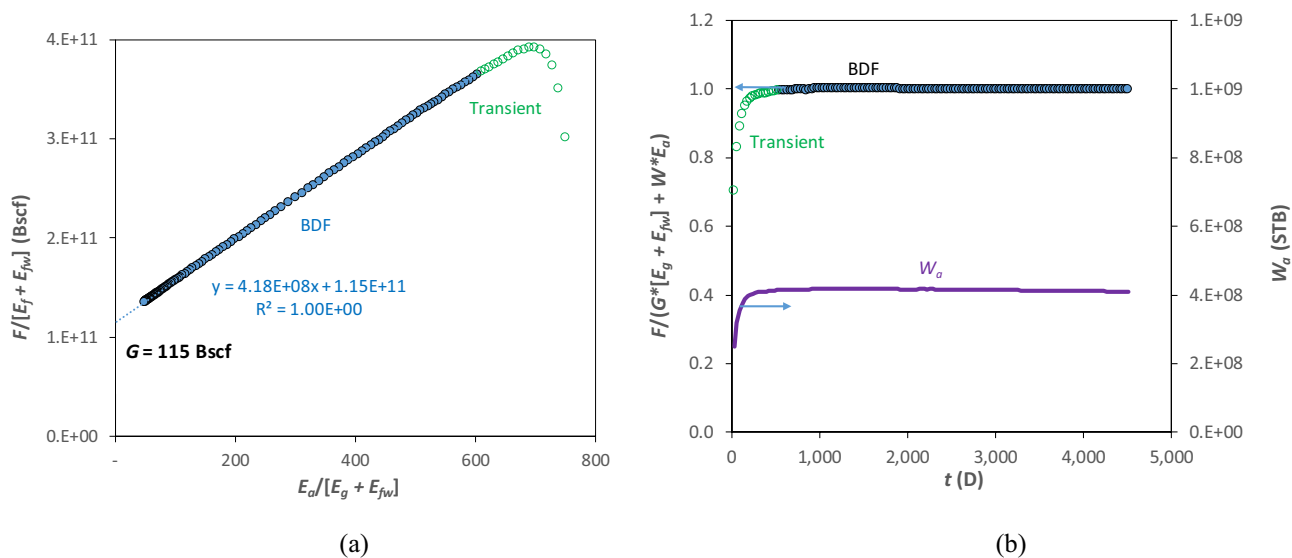
Fig. 5 Material balance for estimating in-place gas volume **a**, and aquifer volume **b** for Example 1
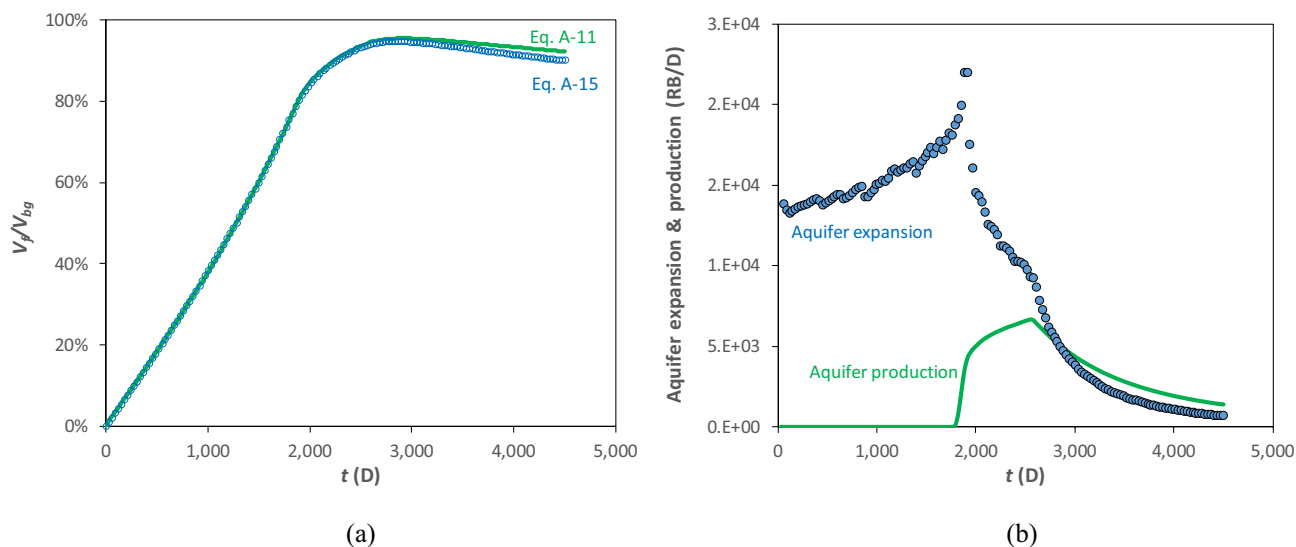

Fig. 6 Dimensionless bulk volumes of a water-influx zone **a**, and aquifer expansion & production **b**; Example 1

one means one-to-one voidage replacement. The diagnostic plot involves two dimensionless variables: pressure (p_{av}/p_i) on the y-axis and volume of water influx, V_f/V_{bg}. Figure 2 displays a plot of (p_{av}/p_i) vs. (V_f/Vb_g), wherein a range of D_{as} values appears. These profiles have the following characteristics:

- For a volumetric gas reservoir, a vertical line @ (V_f/V_{bg}) = 0%; D_{as} = 0, meaning no water influx.

- For a gas reservoir with weak aquifer support, it has an x-intercept @ (p_{av}/p_i) = 0; $0 < D_{as} < 0.5$. When the reservoir gets fully depleted, no water breakthrough occurs.

- For a gas reservoir with strong aquifer support, it has a y-intercept @ (V_f/V_{bg}) = 100%; $0.5 < D_{as} < 1$. When the gas recovery factor (RF) is maximum, there is still energy available in the system.

- For a gas reservoir with infinite aquifer support, it is a horizontal line @ (p_{av}/p_i) = 100%; D_{as} = 1. In other words, no pressure depletion occurs in this case.
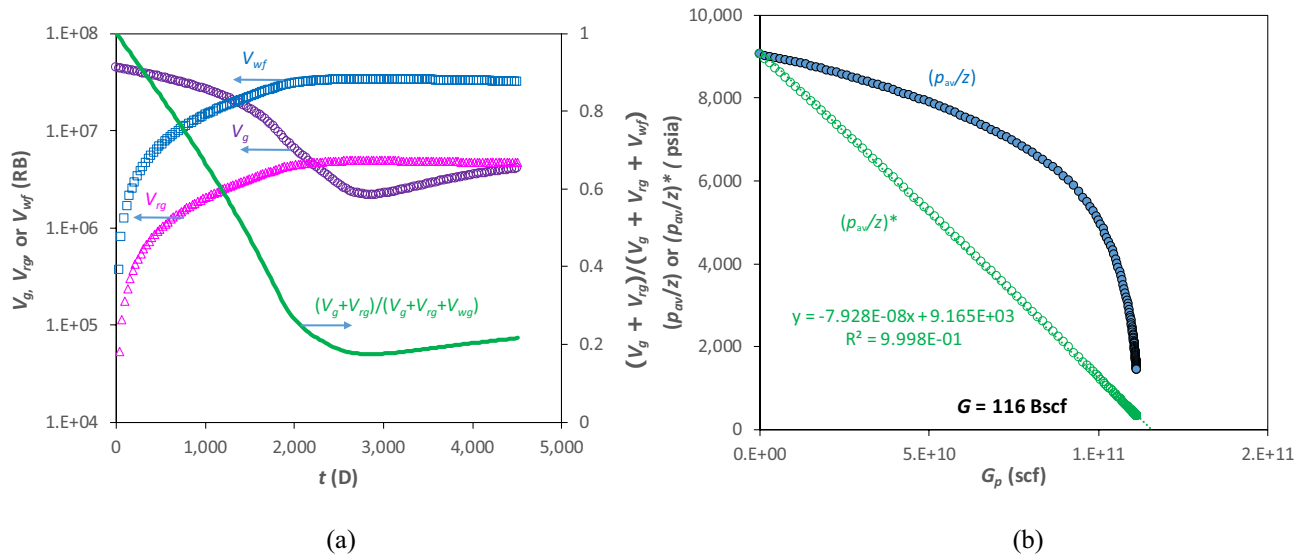
Fig. 7 Estimating volume profiles of gas and water **a**, leading to modified $(p_{av}/z)^*$ plot **b**; Example 1

One can estimate the value of D_{as} as

$$D_{as} = \frac{1}{2}\left(\frac{V_f}{V_{bg}}\right)_{max} + \frac{1}{2}\left(\frac{p_{av}}{p_i}\right)_{@RF_{max}} \tag{19}$$

where

$$\left(\frac{V_f}{V_{bg}}\right)_{max} = \min\left(1, \frac{(c_w + c_f)p_i\left(\frac{V_{ba}}{V_{bg}}\right) - \left(\frac{W_p B_w}{\varnothing_i}\right)\left(\frac{1}{V_{bg}}\right)}{(1 - S_{gr})(1 - c_f p_i) - S_{wi}(1 + c_w p_i)}\right) \tag{20}$$

$$\left(\frac{p_{av}}{p_i}\right)_{@RF_{max}}$$
$$= \max\left(0, 1 - \frac{\left[(1 - S_{wi} - S_{gr}) + \left(\frac{W_p B_w}{\varnothing_i}\right)\left(\frac{1}{V_{bg}}\right)\right]}{p_i\left[(1 - S_{gr})c_f + S_{wi}c_w + (c_w + c_f)\left(\frac{V_{ba}}{V_{bg}}\right)\right]}\right) \tag{21}$$

Figure 3 shows the flowchart of the proposed methodology, which provides a visual representation of the step-by-step process and will help to make the calculation procedure more transparent and accessible.

Model validation and verification

Two synthetic examples validate the modeling approach, and one field example from the literature verifies the proposed method.

Example 1: Synthetic data

The data in this example are from Run #9 of Kabir et al. (2016). This layered Eclipse model has about 198,000 active cells with a cell size of 100 ft × 100 ft × 3 ft. For simplicity and transparency, the model has uniform rock properties. The authors used numerical modeling to generate production data using the following rock and fluid properties in Table 1.

Some of the other relevant attributes of this modeling approach appear in the context of presenting the following example. Production profiles of gas and water (q_g and q_w) and flowing bottom-hole pressure (p_{wf}) appear in Fig. 4. The gas rate remained constant at 50 MMscf/D for about five years without water production. When the well started producing water, the gas rate began to decline. However, the p_{wf} remained stable until about 2000 days before its decline started and reached a minimum value of 1000 psia.

Figure 5a shows the classical material-balance straight-line plot. As expected, the late-time data in the boundary-dominated flow or BDF period appear as a straight line, whereas the early-time transient data do not. The straight line yields the following parameters:

$G = 115$ Bscf; from y-intercept $V_{bg} = 275$ MMRB

$W = 417$ MMSTB; from slope $V_{ba} = 2090$ MMRB

The aquifer is about 7.6 times larger than the gas reservoir relative to the model input value of 10. During transient flow, the values on the left-hand side (LHS) of Eq. 1 are significantly less than those on the right-hand side (RHS). The ratios of (LHS) and (RHS) appear in Fig. 5b. The ratio is less than one during the transient flow period and reaches approximately one during the BDF period. In Eq. 1, using $G = 115$ Bscf, one can estimate the water initially-in-place, W_a. The aquifer volume actively contributes to production
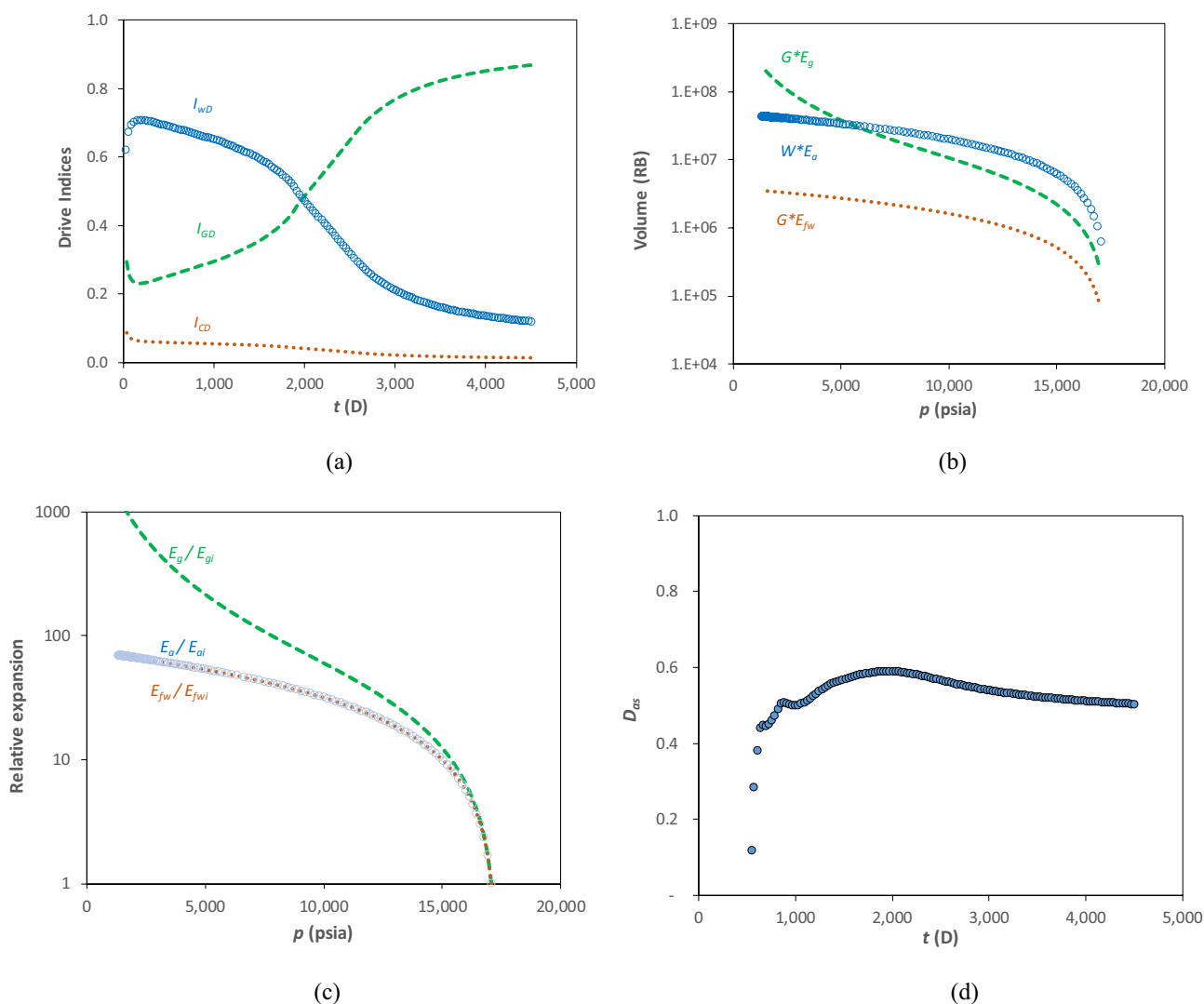
Fig. 8 Drive indices **a**, energy sources **b**, relative expansion factors **c**, and degree of aquifer support **d**; Ex. 1

beyond the transient period. W_a is much less than W during transient flow but increases with time. As expected, W_a equals W during the BDF period when the entire aquifer actively contributes to the production.

Figure 6a shows two bulk volume profiles of the water-influx zone (V_f) in a dimensionless form. The results from these two equations are slightly different. Without any water production, V_f increases monotonically with producing time. Water production begins after about 1800 days, leading to decreasing slope of the profiles. The profile slope is positive if an instantaneous aquifer production rate ($q_w B_w$) is less than the aquifer expansion rate. As Fig. 6b illustrates, after 2830 days of production, $q_w B_w$ becomes more significant than an instantaneous aquifer expansion, causing a declining V_f trend.

Profiles of V_g, V_{rg}, and V_{wf} appear in Fig. 7a. The slope of V_f can explain the individual profiles. While changes in V_{rg}

and V_{wf} are in the same direction as V_f, the V_g trend occurs in the opposite direction. Then, one can calculate a profile of $[(V_g + V_{rg})/(V_g + V_{rg} + V_{wf})]$ for estimating $(p_{av}/z)*$ in Eq. 10. In this case, it declined from 1.0 to around 0.2. Figure 7b shows the profiles (p_{av}/z) and $(p_{av}/z)*$ vs. G_p. A (p_{av}/z) plot is concave downward and yields an overestimated G, especially during early production. At RF = 50%, the (p_{av}/z) plot produces a straight line with R^2 of 0.992, but a G of 375 Bscf, reflecting a 226% overestimation. In other words, the early portion of the (p_{av}/z) plot becomes unsuitable for G estimation. However, with correction, the $(p_{av}/z)*$ resulted in a G of 116 Bscf, close to the input value of 115 Bscf.

Figure 8a shows different drive indices. I_{WD} dominates production at early times, while I_{GD} dominates during the late production period. As expected, I_{CD} is insignificant. Figure 8b displays the production contributions from individual energy sources, and Fig. 8c shows the relative
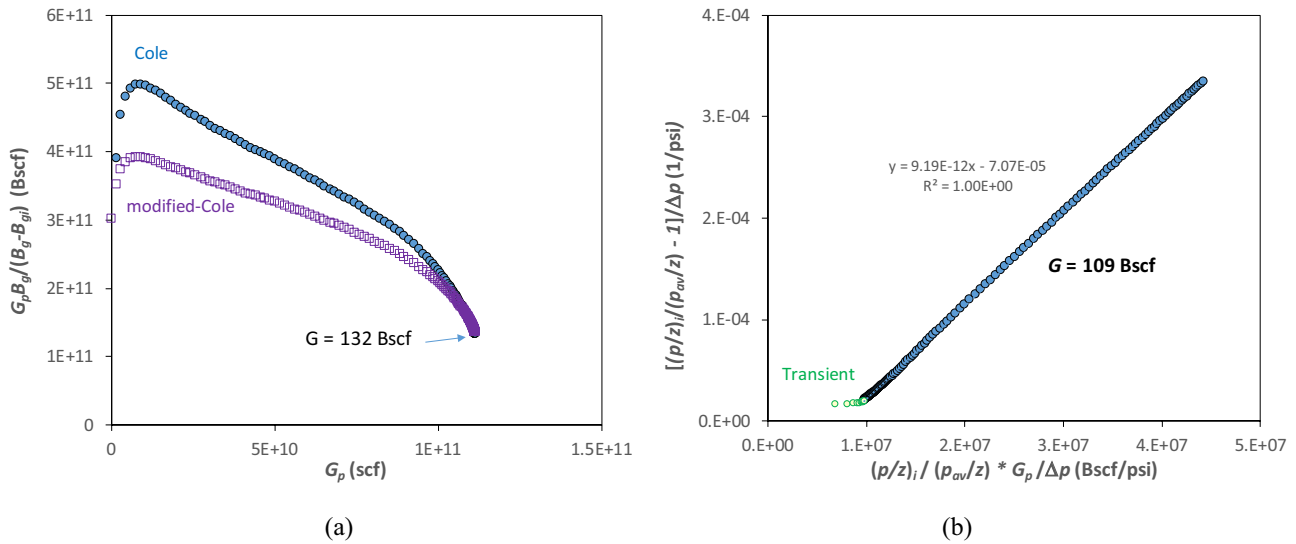
(a)

(b)

Fig. 9 Deriving in-place volume with Cole **a** and Roach **b** plots; Example 1
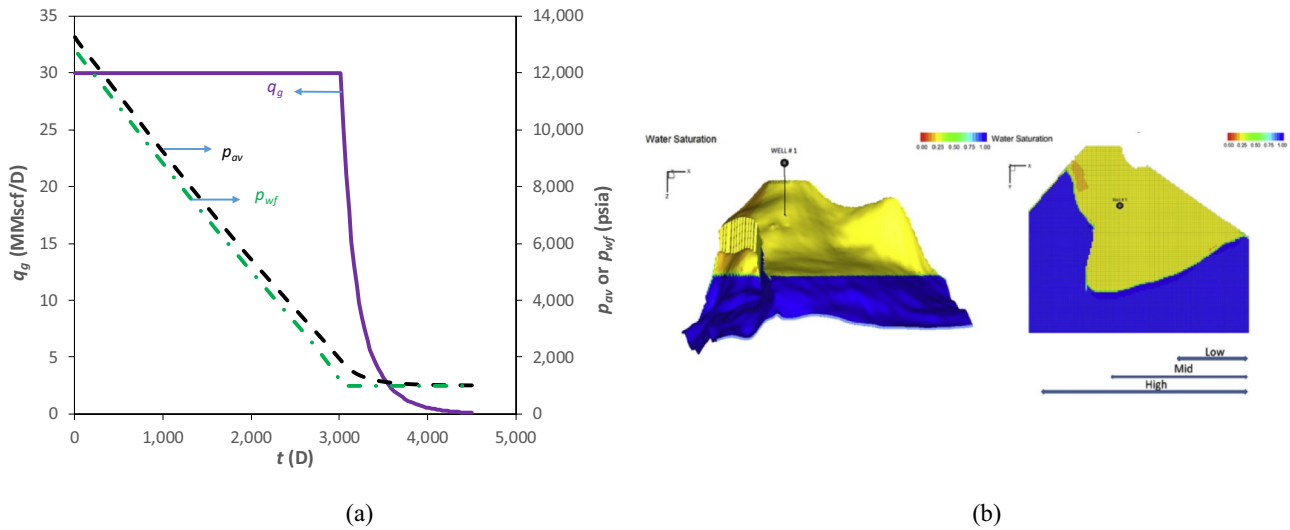

(a)

(b)

Fig. 10 p/q profiles for Ex. 2 **a**, 1/3 aquifer volume (low case) relative to gas may offer delayed energy support **b**

expansion factors. Note that one for the gas drive increases significantly faster than others when depleting the reservoir. The D_{as} profile in Fig. 8d shows that it increases before reaching the maximum during the early production period. When the well starts producing water, D_{as} declines to 0.5. Note that D_{as} is estimated using historical production data only during the BDF period.

Figure 9a shows the results of Cole and modified-Cole plots. The profiles increase very early times and reach a peak before declining. The minimum $G_p B_g/(B_g - B_{gi})$ value is 132 Bscf, and G_p is 111 Bscf. Therefore, the range of G is 111 – 132 Bscf. The result of the Roach (1981) plot appears in Fig. 9b. The value of G is 109 Bscf, derived

from a reciprocal of a slope of the straight line, which is reasonably close to the input value of 115 Bscf.

Example 2: Synthetic data

The data in this example is from Run #15 of Kabir et al. (2016), with an initial pressure of 13,248 psia. The gas rate is kept constant at 30 MMscf/D with declining p_{wf}, as illustrated in Fig. 10a. When p_{wf} reaches 1000 psia, the gas rate starts to decrease. No water production occurred throughout history. The aquifer's size is about one-half of the gas reservoir, as shown in Fig. 10b. The model's left figure reflects the side view, whereas the right represents the top view. This model has 198,000 active cells with uniform rock properties
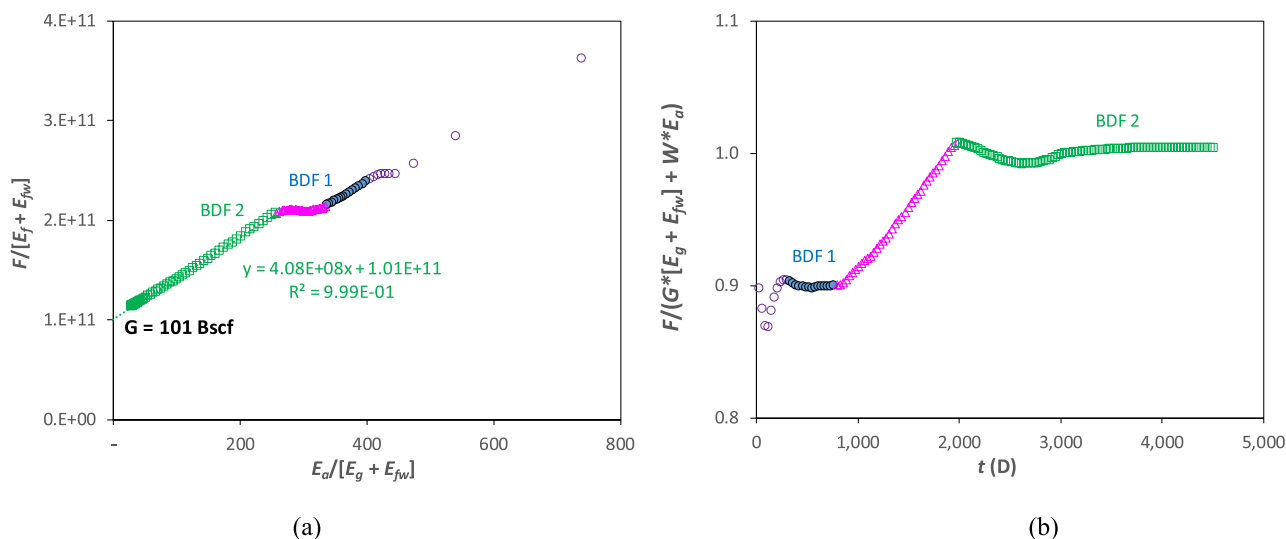
(a)

(b)

Fig. 11 Identification of the flow periods **a** and estimating in-place volume during BDF-2 period **b**; Example-2
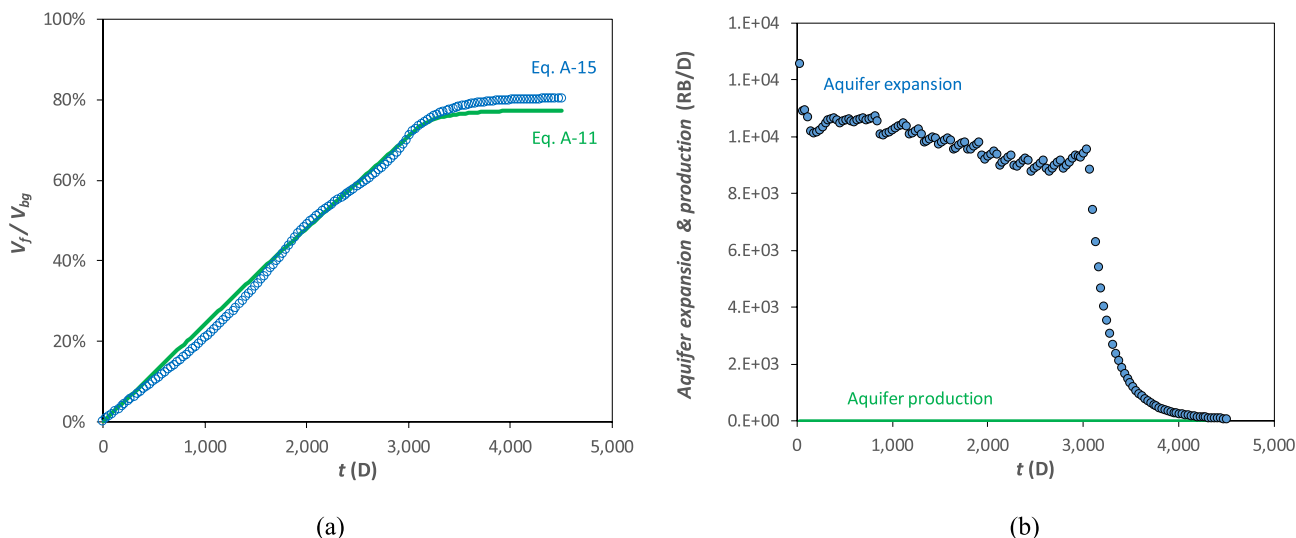

(a)

(b)

Fig. 12 Dimensionless bulk volumes of the water-influx zone **a**, and aquifer expansion and production **b**; Ex. 2

involving 200 md permeability with 20% porosity and water saturation of 20% above the gas/water contact.

Figure 11a shows that two straight lines emerged, given a decreased aquifer volume, and the well's proximity to the aquifer delayed the total system response. The first straight line leads to the following results:

$G = 87.2$ Bscf; $W = 377$ MMSTB, whereas the second straight line yields

$G = 101$ Bscf; $V_{bg} = 316$ MMRB; $W = 408$ MMSTB; $V_{ba} = 2,040$ MMRB

The second straight line corresponds to a more extensive gas–water system. The aquifer size is about 6.5 times larger

than the gas volume. The ratios of the LHS to the RHS of Eq. 1 suggest using values of G and W from the second straight line. The well produces from a smaller reservoir system during BDF-1 than BDF-2.

In the absence of water production, V_f increases monotonically with production time, as Fig. 12a shows. When p_{wf} reaches the minimum, the gas rate starts to decline. V_f reaches the maximum during this period as the aquifer expansion declines, as Fig. 12b illustrates. Figure 6b shows an increasing trend of aquifer expansion during the early flow period, while Fig. 12b shows a decreasing trend. Let us attribute this difference to the two different production periods. A higher production rate causes an increasing pressure
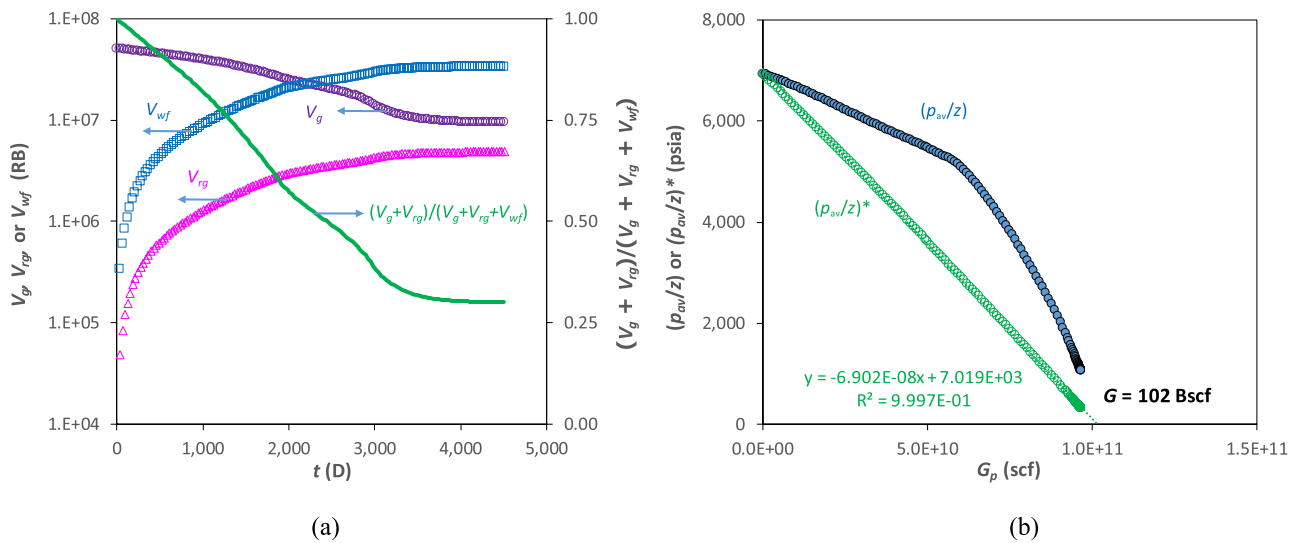
Fig. 13 Tracing volume changes **a** and estimating in-place volume with the modified-$(p_{av}/z)^*$ plot **b**; Example 2
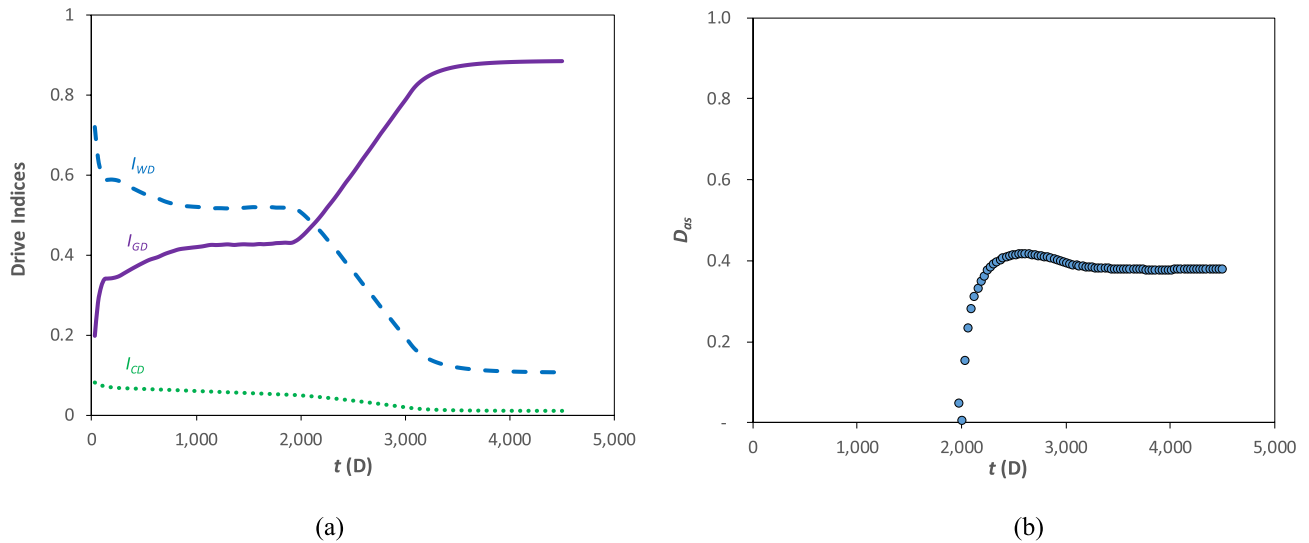

Fig. 14 Drive indices **a** and degree of aquifer support **b**; Example 2

depletion rate, leading to a growing aquifer expansion rate. This reality explains the two BDF periods in Fig. 11.

Figure 13a presents the profiles of V_g, V_{rg}, and V_{wf}. They are all monotonic functions in the absence of water production. The (p_{av}/z) correction factor decreases from 1.0 down to 0.3. On the (p_{av}/z) plot in Fig. 13b, two trend lines emerged, corresponding to two straight lines in Fig. 11a. With the proper correction, $(p_{av}/z)^*$ yields a straight line, with $G = 102$ Bscf.

Figure 14a shows different drive indices. Their behaviors are similar to the ones in Example 1. Figure 14b displays an increasing D_{as} trend at early times, then reaches

the maximum, followed by a decline before stabilizing at a value of 0.38.

Figure 15a shows the results of Cole and modified-Cole plots. The profiles on plots decrease with time, indicating weak aquifer support. The minimum $G_p B_g/(B_g - B_{gi})$ value is 114 Bscf, and G_p is 97 Bscf; therefore, the G range spans 97 to 114 Bscf. The result of the Roach (1981) plot appears in Fig. 15b. The value of G is 102 Bscf, derived from a reciprocal slope of the straight line.

Example 3: Field data

This data from Reservoir A appeared in the study of Rossen (1975). The pertinent reservoir properties appear in Table 2. Figure 16 exhibits a cumulative gas production of
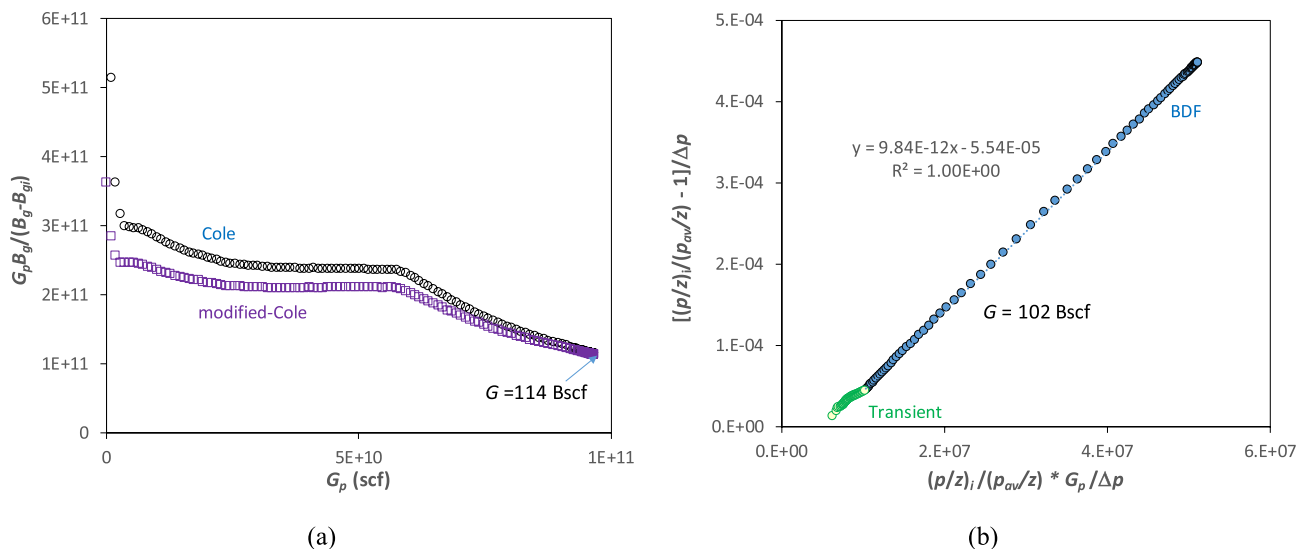
(a)

(b)

Fig. 15 Results of Cole **a** and Roach **b** plots; Example 2

Table 2 Rock and fluid properties for Example 3

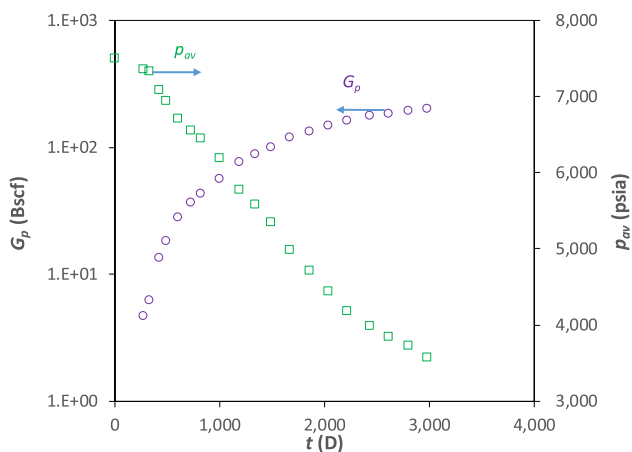| Parameter	Value
p_i, psia	7500
T, ^0F	225
S_{wi}, %	30
Gas SG	0.657

Fig. 16 Production data for Example 3

200 Bscf and a pressure depletion of 3938 psig. No water production appeared in the study.

Figure 17 presents the results of our analysis. The estimated values of G are 417 Bscf from a straight-line plot in Fig. 17a, and 425 Bscf from the proposed $(p_{av}/z)*$ graph in Fig. 17b and W is 1640 MMSTB. The aquifer volume is about five times the gas reservoir.

Figure 18a shows that I_{GD} dominates production for the entire period, given that the aquifer size is insignificant. D_{as} becomes stable after 700 days of production and is slightly less than 0.2, as shown in Fig. 18b.

Figure 19a presents the Cole and modified-Cole plots. Both profiles indicate moderate water drive. The Roach plot in Fig. 19b yields a G value of 431 Bscf. Given the low-D_{as} value of about 0.2, meaning a weak aquifer influx, this G value is close to the other methods shown in Fig. 17.

Discussion

The proposed method for a water-drive gas reservoir overcomes the obstacles that Cole and modified-Cole methods experience. While the Roach method is valid for weak and medium aquifer support, it yields erroneous results when the aquifer support gets stronger. In contrast, the proposed method works well for all degrees of aquifer support, given that it captures the critical mechanisms that are in play in the model. However, the proposed methodology has the following requirements and limitations.

- Besides flow rate, periodic average-reservoir pressure, rock, and fluid properties are essential items.
- The BDF flow period is a requirement.
- Tight reservoirs may have long transient-flow periods and require long shut-in periods to represent the average system pressure.
- The approach may not work for a system with partial communication between the gas reservoir and the aquifer if they operate at different average pressures.
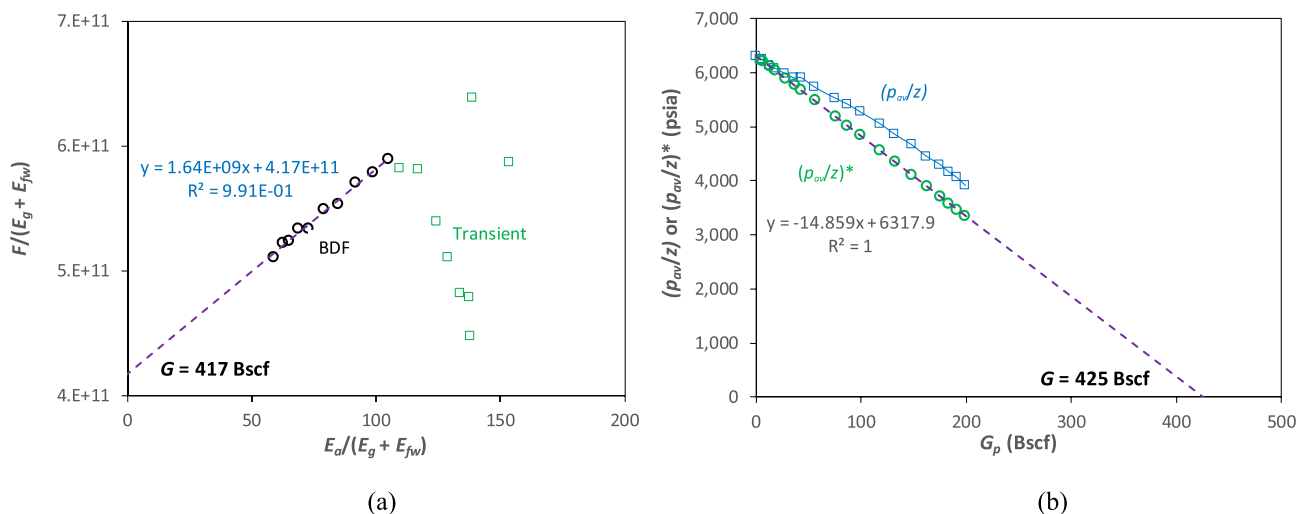
Fig. 17 In-place gas volume estimation with the material-balance **a** and modified-$(p_{av}/z)^*$ methods **b**, Example 3
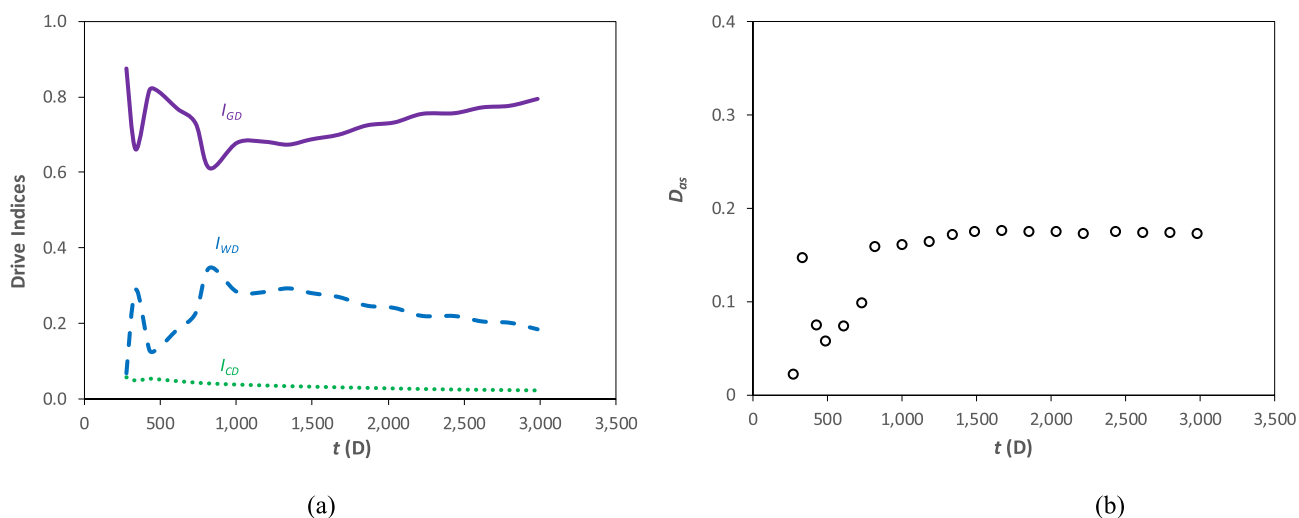

Fig. 18 Drive indices **a** and the degree of aquifer support **b**; Example 3

The proposed method shows that the early production period does not lend itself to a meaningful analysis due to the absence of the boundary-dominated flow (BDF) period. In other words, the whole system does not actively contribute to various production mechanisms during the transient flow period. In this context, the larger the aquifer than the in-place gas volume (V_{ba}/V_{bg}), the longer it takes for the entire production system to reach the BDF due to the increased water-drive index I_{WD}. The degree of aquifer support, D_{as}, as introduced here, measures an aquifer's efficacy. The two field examples showed a range of D_{as} from about 0.2 to 0.4, whereas the two synthetic cases had 0.4 to 0.6, capturing the evolving nature of its trend. In reservoir management, one needs to learn both the aquifer strength (D_{as}) associated with each well and the interwell connectivity through primary capacitance–resistance modeling or PCRM, as shown by Izgec and Kabir (2012). Then, one can adjust withdrawal rates in each reservoir compartment to ensure that premature water breakthrough does not occur. This strategy can assist in maximizing gas recovery.

The increasing aquifer size or the V_{ba}/V_{bg} ratio also adversely impacts the (p_{av}/z) trend on the straight-line plot; the profile with a negative slope signifies the aquifer support. This trend implies that evaluating G from the conventional (p_{av}/z) method will yield an overestimation. In theory, the values of G from the traditional (p_{av}/z) straight-line plot and the modified-$(p_{av}/z)^*$ plot, as introduced here, should be the same in a volumetric system. Application
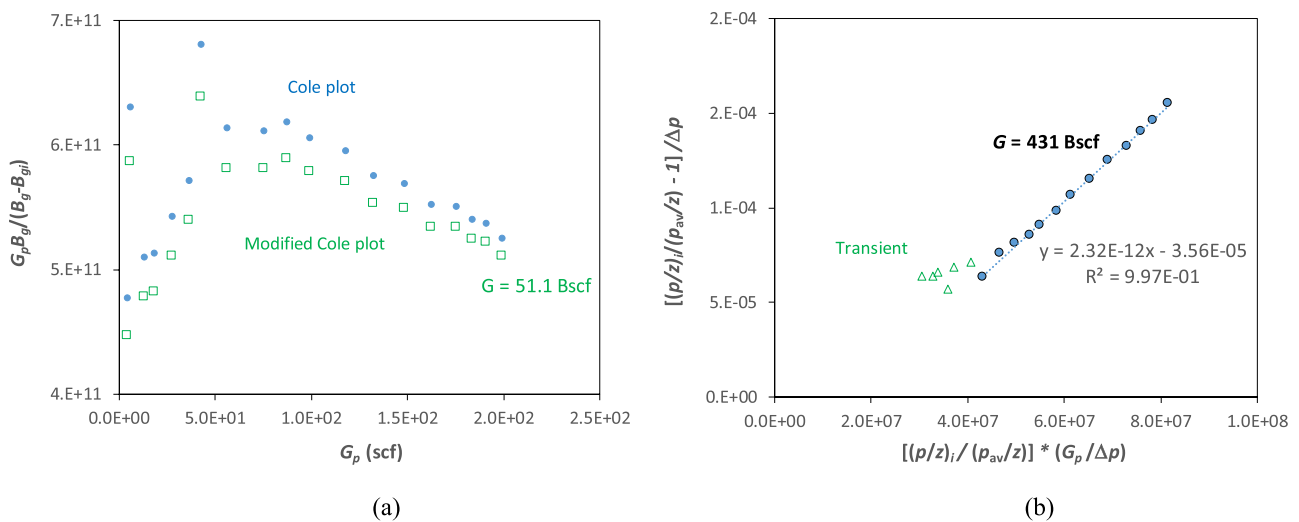
Fig. 19 Results of Cole **a** and Roach methods **b**; Example 3

of the proposed method to analyze production data may yield a difference in these two values. In other words, their difference reflects the uncertainties in G and W. These differences may indicate data quality relating to production data, reservoir pressure, and rock and fluid properties. However, the degree of aquifer influx may be the principal underlying reason. In this context, Brigham's (1997) simplified aquifer model suggests that the pressure change is independent of mobility (k/μ) at each timestep during the BDF period. This reality reassures the estimation of the aquifer volume as presented here.

Studies abound with various forms of rate-transient analysis for estimating in-place gas volume. These methods involve conventional rate-transient analysis (Palacio and Blasingame 1993), dynamic material balance (Mattar et al. 2006), transient-PI (Medeiros et al. 2010), and combined static and dynamic material balance (Ismadi et al. 2012). Those and related studies make serious value propositions in estimating in-place gas volume. Nevertheless, static, and dynamic material-balance methods must objectively arrive at realistic in-place solutions in a water-drive system.

In that regard, our underlying intention focused on exploring the value proposition of estimating both the aquifer and gas in-place volumes to assist the development of numerical models to study the operational strategy in water-drive reservoirs to maximize recovery. That is primarily because all producers experience different degrees of aquifer support, given the variability in the formation permeability and potential geologic baffles leading to the aquifers.

Conclusions

The following conclusions appear pertinent here:

- This study proposes a new methodology to interpret production performance in water-drive-gas reservoirs involving various degrees of aquifer support. Two synthetic datasets verified this method, and one field example provided validation.
- The proposed definition of the degree of aquifer support (D_{as}) quantifies the aquifer strength; it ranges from zero (depletion drive) to one (infinite aquifer support). In this context, the D_{as} values of the three examples spanned from about 0.2 to 0.6. Also, the novel material-balance plot yields a straight line with a slope of W (connected aquifer volume) and a y-Intercept of G (in-place gas). Production data during the early period might not be on a straight line and may have a negative slope, identifying the transient flow period.
- The proposed new plot of $(p_{av}/z)^*$ vs. G_p yields a straight line in a water-drive gas reservoir, similar to a volumetric system's conventional (p_{av}/z) plot. The proposed method estimates the in-place gas volume more accurately than Roach and Cole.

References

Agarwal RG, Al-Hussainy R, Ramey HJ Jr (1965) The importance of water influx in gas reservoirs. J Petrol Tech 17(11):1336–1342. https://doi.org/10.2118/1244-PA

Brigham WE (1997) Water influx and its effect on oil recovery: Part 1. Aquifer flow. Technical report, SUPRI TR 103, Contract No. DE-FG22-93BC14994, US DOE/Stanford University, Stanford, California, USA

Bruns JR, Fetkovitch MJ, Meitzen VC (1965) The effect of water influx on p/z−cumulative gas production curves. J Petrol Tech 17(3):287–291. https://doi.org/10.2118/898-PA

Campbell RA, Campbell JM Sr (1978) Mineral property economics, vol. 3: petroleum property evaluation. Campbell Petroleum Series, Norman, Oklahoma, USA

Chierici GL, Pizzi G, Ciucci GM (1967) Water drive gas reservoirs: uncertainty in reserves evaluation from past history. J Petrol Tech 19(2):237–244. https://doi.org/10.2118/1480-PA

Cole FW (1969) Reservoir engineering manual, 285. Gulf Publishing Co, Houston, Texas

Dake LP (1983) Fundamentals of reservoir engineering. Elsevier Scientific Publishing Co., Amsterdam, pp 29–33

El-Ahamady M, Wattenbarger RA (2007) A straight-line p/z plot is possible in waterdrive gas reservoir. Paper SPE 103258 presented at the SPE Rocky Mountain Oil & Gas Technology Symposium, Denver, Colorado, U.S.A. 16–18 April

Havlena D, Odeh AS (1963) The material balance as an equation of a straight line. J Petrol Tech 15(8):896–900. https://doi.org/10.2118/559-PA

Hurst W (1943) Water influx into a reservoir and its application to the equation of volumetric balance. Trans AIME 151(1):57–72. https://doi.org/10.2118/943057-G

Ismadi D, Kabir CS, Hasan AR (2012) The use of combined static- and dynamic-material-balance methods with real-time surveillance data in volumetric gas reservoirs. SPE Res Eval Eng 15(3):351–360. https://doi.org/10.2118/145798-PA

Izgec O, Kabir CS (2010) Quantifying nonuniform aquifer strength at individual wells. SPE Res Eval Eng 13(02):296–305. https://doi.org/10.2118/120850-PA

Izgec O, Kabir CS (2012) Quantifying reservoir connectivity, in-place volumes, and drainage-area pressures during primary depletion. J Petrol Sci Eng 81 (2012):7–17 http://dx.doi.org/j.petrol.2011.12.015

Kabir CS, Parekh B, Mustafa MA (2016) Material-balance analysis of gas and gas-condensate reservoirs with diverse drive mechanisms. J Nat Gas Sci Eng 32(2016):158–173. https://doi.org/10.1016/j.jngse.2016.04.004

Kazemi N, Ghaedi M (2020) Production data analysis of gas reservoirs with edge aquifer drive: a semi-analytical approach. J Nat Gas Sci Eng 80(2020):103382. https://doi.org/10.1016/j.jngse.2020.103382

Mattar L, Anderson D, Stotts GG (2006) Dynamic material-balance-oil or gas-in-place without shut-ins. J Can Petrol Tech 37(2):52–55. https://doi.org/10.2118/06-11-TN

McEwen CR (1962) Material balance calculations with water influx in the presence of uncertainty in pressures. SPE J 2(2):120–128. https://doi.org/10.2118/225-PA

Medeiros F, Kurtoglu B, Ozkan E, Kazemi H (2010) Analysis of production data from hydraulically fractured horizontal wells in shale reservoirs. SPE Res Eval Eng 13(03):559–568. https://doi.org/10.2118/110848-PA

Moghadam S, Jeje O, Mattar L (2011) Advanced gas material balance in simplified format. J Can Petrol Tech 50(1):90–98. https://doi.org/10.2118/139428-PA

Palacio JC, Blasingame TA (1993) Decline-curve analysis using type curves-analysis of gas well production data. Paper SPE-25909-MS presented at the Rocky Mountain Regional/Low-Permeability Reservoirs Symposium and Exhibition, Denver, Colorado, USA, 26–28 April. https://doi.org/10.2118/25909-MS

Pletcher JL (2002) Improvements to reservoir material-balance methods. SPE Res Eval Eng 5(1):49–59. https://doi.org/10.2118/75354-PA

Roach RH (1981) Analyzing geopressured reservoirs–a material balance technique. Paper SPE 9968 available from SPE, Richardson, Texas

Rossen RH (1975) A regression approach to estimating gas in place for gas fields. J Petrol Tech 27(10):1283–1289. https://doi.org/10.2118/5062-PA

Schilthuis HJ (1936) Active oil and reservoir energy. Trans AIME 118(1):33–52. https://doi.org/10.2118/936033-G

Tehrani DH (1985) An analysis of a volumetric balance equation for calculation of oil-in-place and water influx. J Petrol Tech 37(9):1664–1670. https://doi.org/10.2118/12894-PA

van Everdingen AF, Hurst W (1949) The application of the Laplace transformation to flow problems in reservoirs. J Petrol Tech 186:305–324. https://doi.org/10.2118/949305-G

Vega L, Wattenbarger RA (2000) New approach for simultaneous determination of the OGIP and aquifer performance with no prior knowledge of aquifer properties and geometry. Paper SPE-59781-MS presented at the 2000 SPE/CERI Gas Technology Symposium, Calgary, Alberta, Canada, 3–5 April. https://doi.org/10.2118/59781-MS

Wang B, Teasdale TS (1987) GASWAT-PC: A microcomputer program for gas material balance with water influx. Paper SPE-16484-MS presented at the SPE Petroleum Industry Applications of Microcomputers, Montgomery, Texas, 23–26 June. https://doi.org/10.2118/16484-MS

Yildiz T (2008) A hybrid approach to improve reserves estimates in waterdrive gas reservoirs. SPE Res Eval Eng 11(4):696–706. https://doi.org/10.2118/99954-PA

Yildiz T, Khosravi A (2007) An analytical bottomwaterdrive aquifer model for material-balance analysis. SPE Res Eval Eng 10(6):618–628. https://doi.org/10.2118/103283-PA

Yu Q, Hu X, Liu P et al (2019) Research on calculation methods of aquifer influx for gas reservoirs with aquifer support. J Petrol Sci Tech 177(2019):889–898. https://doi.org/10.1016/j.petrol.2019.03.008

Zaremoayedi F, Ghaedi M, Kazemi N (2022) A new approach to production data analysis of non-volumetric naturally fractured gas-condensate reservoirs. J Nat Gas Sci & Eng 105:104703. https://doi.org/10.1016/j.jngse.2022.104703